PAPER NUMBER

132

CORROSION 90

April 23-27, 1990 · Bally's Hotel, Las Vegas, Nevada

ELECTROCHEMICAL IMPEDANCE OF CORROSION MACROCELLS ON REINFORCING STEEL IN CONCRETE

Alberto A. Sagüés
Department of Civil Engineering and Mechanics
University of South Florida
Tampa, Florida 33620

ABSTRACT

Macroscopic corrosion cells (macrocells) on reinforcing steel in concrete were investigated by electrochemical impedance spectroscopy (EIS) measurements. Segmented steel bars with individual electrical connections were cast in concrete slabs. The slabs were placed vertically in a sodium chloride solution so that only the lower portion was in contact with the liquid. The lower portions of the bars became anodes, while the upper portions acted as cathodes where oxygen reduction was predominant. The macrocell currents flowing between elements of each bar were monitored externally. EIS measurements were made using entire bars or individual segments as working electrodes. In the latter case, high-impedance current sources were used to provide a.c. isolation between the segment tested and the rest of the bar. Highly differentiated behavior was observed between cathodic and anodic areas. Segments where oxygen reduction was predominant provided results that suggested that the reaction was activation-limited in relatively dry concrete. A model was formulated and applied to predict the EIS response of the entire bar based on the behavior of individual segments.

Keywords: concrete, corrosion, impedance, macrocell, rebar, reinforcing, steel, electrochemical, methods, oxygen, polarization, marine, cement, current.

INTRODUCTION

In a simple corrosion macrocell, the cathodic and anodic reactions may be considered to take place at distinct, macroscopically separated regions on the surface of a metallic body. Both regions are in contact with the same electrolyte. If the electrolyte has finite resistivity, the potential of the metal (with respect to a reference electrode placed immediately adjacent to the metal surface) will be different at the cathodic and anodic regions. If an external source impresses a current on the metallic body, a resulting variation in potential will take place. The measured value of the potential deviation will depend on the placement of the sensing reference electrode, and on the physical configuration of the counter electrode used

to impress the current. Thus, polarization measurements such as Electrochemical Impedance Spectroscopy (EIS) will be convoluted by the distribution of the macrocell reactions and by the arrangement of the measuring system electrodes. These effects are likely also to by frequency-dependent [1].

EIS measurements are being increasingly used to characterize corrosion in systems involving complex macrocell action. This is the case of corrosion of reinforcing steel bars (rebars) in concrete, where polarization techniques are used to non-destructively obtain information on the corrosion condition of the system. However, because of the complicating factors mentioned above, interpretation of the EIS response is often difficult. This paper will address the predicted response of a corrosion macrocell with attention to evaluating the corrosion behavior of steel in concrete from EIS measurements.

Reinforcing steel in freshly cured concrete is normally passive because of the high pH of the concrete pore fluids. However, the steel environment may change adversely due to external contamination. In a common form of deterioration, chlorides from seawater or road deicing salts penetrate the concrete cover and cause depassivation of the steel [2]. Corrosion is thus initiated, with oxygen reduction often being the corresponding cathodic reaction. The location of the oxygen reduction reaction is determined by many factors, including the permeability of the concrete cover, the availability of oxygen at the concrete surface, and the resistance of the electrolytic macrocell paths involved. In this type of system, polarization measurements are expected to be complicated by the current distribution and differential electrochemical excitation effects mentioned above. To obtain an indication of the factors affecting the electrochemical impedance response, the next section will address the case of an idealized discrete corrosion macrocell possessing some of the characteristics of the extended configuration that is encountered in an actual system.

The Discrete Macrocell

Figure 1 shows schematically the main components of the corroding system to be examined. The metal is considered to have negligible electrical resistance. Electrode reactions and contact with the electrolyte are assumed to take place only at regions 1 and 2, which will be considered as separate points. The electrical characteristics of each of these regions will be modelled in terms of a d.c. voltage source E_i in series with a small-signal polarization impedance Z_i (which has the form of a complex vector). The electrolyte connecting regions 1 and 2 is assumed to be distributed along one dimension and having purely ohmic characteristics, with a total resistance $R = R_a+R_b$. The potential at points of the electrolyte facing regions 1 and 2 is V_1 and V_2 respectively, referred to the metal. A discrete counter electrode is placed at point 3 in the electrolyte, where a low-amplitude excitation current described by the complex vector I_s applied by an a.c. current source. Prior to applying I_s the current circulating through the electrolyte was the macrocell current $I=(V_1-V_2)/R$. Application of I_s will change the current across R_a to $I+I_a$ and that across R_b to $I+I_b$. The potentials at points 1, 2 and 3 will change to V_1+V_a, V_2+V_b and V_3+V_c respectively (I_a, I_b, V_a, V_b and V_c are also complex vectors). Current and potential balance for the circuit's nodes and loops yields the following small-signal relationships:

$$I_a+I_s=I_b \qquad (1)$$

$$V_a=-Z_1\ I_a \qquad (2)$$

$$V_b = Z_2 \, I_b \qquad (3)$$

$$V_a - V_b = R_a \, I_a + R_b \, I_b \qquad (4)$$

Equations (1) to (4) can be solved to provide the relationship between the excitation current and potential change at all nodes of the circuit. In an experimental setup, the potential changes measured will be those present at the point where the reference electrode is placed. The impedance measured, Z_m, will be given by the ratio of that potential change to the impressed current (this is valid whether the measurements are conducted galvanostatically or potentiostatically). If the reference electrode is placed near one of the components of the macrocell, for example near point 1, the impedance measured at point 1, Z_{m1}, will be:

$$Z_{m1} = Z_1 Z_2 / (R_a + R_b + Z_1 + Z_2) + R_b Z_1 / (R_a + R_b + Z_1 + Z_2) \qquad (5)$$

If $R_a, R_b \to 0$ then $Z_{m1} \to 1/(1/Z_1 + 1/Z_2)$ which is the parallel combination of the impedance of both elements of the macrocell, as expected from general principles [3]. If $R_a \to 0$ and $R_b \to \infty$ then $Z_{m1} \to Z_1$ and the measured value will be that of the macrocell half closest to the counter and sensing electrodes. If $R_b \to 0$ and $R_a \to \infty$ (sensing electrode at the opposite end from the counter electrode in a long macrocell) then Z_{m1} is vanishingly small. These extreme cases indicate the wide range of results that can be obtained when performing polarization tests in an extended macrocell.

Continuous Macrocells

The analysis above can be extended to a metallic body of finite dimensions in contact with an electrolyte, where each element of the metal surface has its own interfacial impedance [3] (which is the result of interactions with other parts of the system). Conversely, a continuous system may be discretized into macroscopic elements keeping in mind that increasingly larger modeling errors will arise as larger elements are used. If the individual response of each element is known (from previous measurement or predictions), then the impedance of the entire component measured under specified conditions could be predicted. This procedure could in principle be reversed if enough additional information is known about the system (for example electrolyte resistance distribution and polarization properties of the material), and the impedance response could then be at least partially deconvoluted to evaluate the extent of corrosion at individual areas.

Macrocells in reinforced concrete

The resistivity of hardened concrete ranges from values on the order of 500 ohm-cm for porous, wet concrete to virtually unmeasurably high values under very dry conditions [4]. This resistivity can give rise to significant potential drops between primarily cathodic and anodic areas, creating a complicated system response when electrochemical measurements are attempted. Marine bridge substructure members have the additional complication of an extended conductivity gradient from the lower regions in contact with sea water to often very dry portions near the deck. Evaporation patterns also cause accumulation of chlorides in the area just above the high water mark. This tends to cause the steel there to depassivate first, but changing conditions may shift the area of maximum corrosion to other parts of the column. The reinforcing steel bars can be several meters long, and complicated macrocell patterns can develop [5].

In an investigation aimed at developing information on the development of corrosion

under partial submersion conditions, reinforced concrete slabs with multiple reinforcing steel elements were exposed for over two years to liquids containing various amounts of chloride [5]. The steel elements were fitted with external electrical connections that allowed individual and collective measurements of electrochemical response. This paper will describe the results of electrochemical impedance measurements in a selected group of specimens. The results will be interpreted by means of a discretized model where the combined response of the macrocell will be predicted based on the response of individual elements.

EXPERIMENTAL

The reinforced concrete specimens were slabs 45 cm high, 15 cm wide and 5 cm thick (18 X 6 X 2 inches) containing rebars placed parallel to the longest dimension. The bars, 9 mm (3/8 inch) in diameter, were either one-piece or divided into separate segments. The length of bar exposed to concrete was 11.5 cm each for the top and bottom segments and 4.0 cm each for the two middle ones. Each rebar or segment had its own independent external electrical connection. External switches and contacts were used to connect segments with each other as desired. The arrangement permitted the measurement of intersegment currents, polarization characteristics of whole bars or individual segments, and the ohmic resistance of the concrete between bars or segments. The segmented bars were kept with all the switches between segments either normally closed (NC) or normally open (NO) through the experiment. The multi-element bars exposed under those conditions will be hereafter designated NC bars and NO bars, respectively. The different bar and segment combinations used and their normal switching condition are shown with dimensions in Figure 2. Activated titanium reference electrodes, 3mm in diameter and 5 cm long (1/8 X 2 inches) were embedded halfway between the bars at four locations as shown in Figure 2.

The bars were made of low carbon (typically 0.04 % C) steel of the type used for welded-wire reinforcement for concrete culverts. The surface of the steel was sandblasted to a white metal finish. Consecutive segments were separated from each other by a metallographic-mount epoxide plug which was cast in place. The plug served also to isolate the junction between rebar and external connecting cable from the concrete environment.

The slabs were made using concrete with a 0.5 water-to-cement ratio, with slump of 7.5 cm. The concrete mix used Type 1 cement, with coarse and fine aggregates as per the standard Florida Department of Transportation test mix design [5]. After casting, the slabs were moist-cured for 28 days. Following curing the specimens were placed standing so that the bottom 17.5 cm (7 inches) were submerged in water. The impedance experiments described here were performed with specimens that were exposed to water containing either 300 or 9000 ppm chloride (from dissolved NaCl) for over 900 days. The water pH was kept at 8.5 by means of a controlled pump that delivered fresh solution upon demand. The laboratory temperature was 21°C, and the air relative humidity was typically 65%. Detailed descriptions of the experimental arrangement, which included separate tests of slabs exposed to several other water chemistries, are given in references [5] and [6].

As a result of the exposure conditions, the moisture content of the concrete varied from water saturation in the submerged region, to very dry concrete at the top of the slab. This in turn influenced the chloride distribution along the specimen. Figure 3 from data in reference [5] illustrates the composition profiles observed in a specimen exposed for 300 days to the 9000 ppm chloride environment. Notable is the

chloride accumulation in the zone just above the waterline, resulting from capillary transport and evaporation of the chloride rich liquid. This pattern is commonly observed in bridge substructure members [7] as well as in laboratory tests [8].

EIS measurements were performed using current control and measuring the corresponding potential response. The working electrode was an entire rebar or a rebar segment. If the rebar segment was in a NO array, it was tested in that condition. If the segment was part of a NC array, the segment was separated from the others by opening the necessary switch or switches. However, to preserve the segment's static polarization condition high impedance DC current sources were connected across each open switch. The sources were adjusted to exactly reproduce the closed-switch circuit macrocell currents. The current sources were small and highly stable battery operated circuits as shown in Figure 4. The value of the source resistor Rs was typically two orders of magnitude greater than the highest impedance vector measured in the segment. Thus, the measured segment impedance was virtually unaffected by that of the other segments in the same array. The reference electrode used was the internal embedded one next to the segment to be tested. The counter electrode was the other parallel bar or segment of bar existing in the same slab. Sketches next to the EIS data detail the electrode configuration used in each experiment.

The apparatus used to obtain the EIS measurements has been described elsewhere [9]. Deviations form the corrosion potential were kept typically to less than 10 mV. A Faraday cage was used in most experiments to keep the reinforced concrete specimen free from external electrical noise.

RESULTS

Potentials and Interelectrode Current Patterns

Three multi-element reinforced concrete slabs were selected (from a total matrix of 12 instrumented slabs) for detailed EIS measurements. One of the slabs, designated P1, was constructed as in Type 1 of Figure 2 and exposed to a liquid of 1000 ohm-cm resistivity, pH of 8.5 and a chloride concentration of 300 ppm. Figure 5 shows the evolution with time of the electrode potential of the steel elements in the slab. All potentials are with respect to an SCE immersed in the liquid. Independent curves correspond to each of the elements in the NO bar, while the evolution of potential in the NC bar is represented by a single curve. All potentials remained high through the 900-day test, indicating that the steel surface remained passive during the exposure period. The magnitudes of electrical currents between elements joined by switches in the NC bar remained below 0.5 uA throughout the test period.

The remaining two slabs, designated A1 and A2, where configured as in Types 1 and 2, respectively, in Figure 2. Both slabs were exposed to a liquid with 35 ohm-cm resistivity, pH =8.5 and 9,000 ppm chloride. The electrode potential vs time behavior for one of those slabs (A1) is shown in Figure 6 using the earlier format. The downward potential transitions suggest that active corrosion had developed in various elements of that slab, beginning at about 100 days of exposure. The magnitude of the electrical currents between elements joined by NC switches increased dramatically coincident with the observation of the potential transitions. The highest interelement currents were on the order of 10 uA. The currents experienced long-term variations reflecting the establishment of corrosion macrocell patterns. In most cases the direction of the current corresponded to a net flow of electrons from the lower to the upper elements. The values of the currents at the time EIS measurements were taken

are given starting in Figure 10.

Interelement Ohmic Resistances

Figure 7 shows schematically the results of measuring the point-to-point resistance between elements and/or bars in slabs P1, A1 and A2 with all switches open. All measurements were taken with an AC ohmmeter that used a low-amplitude, 12 Hz square wave signal as the excitation current. The measurements shown were obtained within a single day during the period when EIS tests were performed. The resistances corresponding to the elements in dryer concrete (especially in Slabs A1 and A2) were observed to be sensitive to small variations in ambient laboratory conditions.

EIS Measurements, Slab P1

Figure 8A summarizes the EIS behavior measured on the NC bar, connected as a working electrode, when selecting pairs of counter/reference electrodes at the four available levels. The connection scheme for each test is identified in the sketch next to each impedance diagram. As shown, each independent element of the opposite NO bar was used in turn as a counter electrode in combination with the closest reference electrode. All switches were in their normal configuration during the measurements.

Figure 8B shows the EIS results when each independent element in the NO bar was used as a working electrode. All switches in the NO bar remained open during the tests. The reference electrode in each case was the closest to the element being measured. The counter electrode was the NC bar in its normal configuration.

For brevity, only the impedance diagram (Nyquist plot) is shown for each test. When represented in Bode format, the data in Figures 8 had the typical appearance exemplified in Figure 9. In this representation the low frequency impedance magnitude data approached a straight line in each case. The slope of the line varied between 0.8 and 0.95, with the highest values corresponding to the lower three elements in the NO bar. The high frequency plateau of the impedance magnitude was used to define a nominal electrolyte resistance for each test. The resulting value is indicated in parenthesis at each impedance diagram in the corresponding Figure for this and the other slabs.

EIS measurements, Slab A1

Figure 10A shows impedance measurements performed on the NC bar in its normal configuration while using, in turn, increasingly higher elements of the NO bar as counter electrodes (all NO bar switches remained open during the tests). The nearest reference electrode was used in each case. The small upturn at the highest test frequencies (1KHz to 10 KHz) in the upper plot resulted from parasitic wiring capacitances, which affected the readings when measuring impedances of high magnitude. Figure 10B shows measurements performed using the same combinations of counter and reference electrodes as in Figure 10A, but this time each element being tested in the NC bar was a.c.-isolated from the rest during its test by high impedance current sources. The value and the electronic direction of the balancing currents are shown in each connection schematic.

Figure 11 shows the results of EIS measurements obtained when using as working electrodes each of the separate elements in the NO bar. The nearest reference electrode was used in each case. The counter electrode was the entire NC bar with all switches closed.

EIS Measurements, Slab A2

Figure 12A shows EIS measurements performed with the NC bar as the working electrode (all switches closed). The other bar, which was physically continuous, was used as the counter electrode. The tests differed only in the position of the reference electrode. Figure 12B shows measurements performed with the same reference and counter electrode arrangements as in Figure 12A, but this time each individual element in the NC bar was a.c.-isolated from the rest during its test by high impedance current sources. The corresponding electronic currents are shown in each case.

DISCUSSION

Corrosion Behavior and Macrocell Configuration

The trends observed in the electrode potentials and interelement currents are as expected from the slab configuration and the liquid chemistries used. As shown in Figure 3, high chloride contents can develop by evaporation at the region near the water line. If the chloride content of the liquid is high enough (as in the case of slabs A1 and A2), the chloride threshold for active corrosion initiation is reached after a relatively short time of exposure. The onset of active corrosion is manifested by a drop of several hundred mV in the electrode potential.

The most likely cathodic reaction in concrete exposed to the atmosphere is the reduction of oxygen, which must reach the surface of the metal by transport through the concrete cover. The effective diffusion coefficient of oxygen through concrete is greatly reduced by moisture (the value can be two orders of magnitude lower in a 100% relative humidity environment than under 60% relative humidity conditions [10]). Because corrosion is initiated in an area of high chloride content but also relatively high water content, the cathodic reaction is likely to take place preferentially upward in the bar where oxygen is more available. The metal there is still passive because the chloride content is low. As a result, a corrosion macrocell is formed. Metal dissolution is predominant at the chloride enrichment zone, oxygen reduction at the dryer upper portion, an upward electronic current flows through the metal, and a matching ionic current flows through the body of the slab.

All the full length electrically continuous bars (both segmented and in one piece) in slabs A1 and A2 showed a sharp potential drop early during the exposure period, indicating that the critical chloride content for corrosion initiation had been reached somewhere in the bar. The pattern of currents described above is observed in the NC bars in slabs A1 and A2 (as shown starting in Figure 10). The electronic currents are in the upward direction. In both cases the highest element is a net electron consumer, sinking a sizable current even though the concrete conductance was relatively small in that region (see below). The current distribution shows that in slab A1 (Figure 10) the element just above the water line is the greatest net electron generator, suggesting that anodic action is highest there. That role is played in slab A2 by the element below the water line (Figure 12).

The potential of the independent elements of the NO bar in Slab A1 (Figure 6) show the evolution with time that could be expected when extended macrocell currents cannot flow. The highest element, low in chlorides, remained passive through most of the test period. The other elements experienced downward potential transitions at times consistent with the chloride accumulation trends: early in the element just

above the water line, and later for the one fully submerged and for the one at an intermediate height above water. Similar trends were observed in another specimen exposed to the same environment and reported elsewhere [5].

In slab P1 the low chloride environment did not promote enough chloride accumulation in the concrete for the development of active corrosion. All potentials remained high through the exposure (Figure 5). Interelectrode currents in the NC bar were negligible.

The ohmic measurements shown in Figure 7 agree with the expected moisture and chloride distribution patterns. The resistances between points at the highest elements were the greatest, while low resistances were measured in the submerged zone. The point-to-point resistances measured include not only the contribution of the concrete immediately between the element pairs, but also that of the conduction paths of adjacent concrete and liquid zones. As a result, the actual conductance between pairs of segments at a given level is always less than could be inferred from the values indicated. Conversion of the results to an equivalent network of interelectrode conductances has been attempted. Preliminary results indicate that the concrete resistivity at the water immersed area is on the order of 1000 ohm-cm. At the top level of slab P1 the estimated average resistivity is on the order of 1 M ohm-cm.

EIS Behavior, Passive Conditions.

The impedance diagrams for slab P1 (Figure 8), where active corrosion did not take place, show the behavior generally observed in passive steel in concrete [1,11]. The isolated segments in the lower part of the NO bar showed predominantly capacitive behavior, as evidenced in Figure 9 by the near-unity slope of the low frequency portion of the impedance magnitude Bode plot [12]. Assuming that the behavior observed in the NO bar is solely the result of interfacial capacitance, an equivalent value C for that magnitude can be calculated from

$$C=A/2\pi f\,(-\mathrm{Im}(Z)) \qquad (6)$$

where A is the apparent area of metal in contact with the electrolyte, f is the test frequency and Z the measured impedance. Using the results from the lowest test frequency, one obtains values of 130, 100, 160 and 180 uF/cm^2 for the elements in the NO bar (starting from the top). The segments in the NC bar form a composite electrode that shows also a high phase angle behavior at the four elevations tested (Figure 8A). The magnitude of the imaginary component of the impedance at the lowest frequency tested is about the same in all four cases. The corresponding nominal interfacial capacitance, using an analysis similar to that for the NO bar, is an average of 120 uF/cm^2. These values are comparable with others obtained in an investigation [13] of sandblasted steel without corrosion products in an alkaline environment. Interestingly, the apparent interfacial capacitance does not seem to vary significantly for the elements at different heights in the NO bar, even though the concrete resistivity changes over two or more orders of magnitude.

The effective working-to-reference electrode resistance is higher for the tests involving elements further away from the water. The values of this resistance are a fraction (roughly 1/3) of the point-to-point resistances shown in Figure 7 for matching elements in the slab. This is to be expected since the reference electrodes are placed halfway between the element pairs. The magnitude of the interfacial impedances of individual segments in the NO bar is relatively high (at least at the lowest frequencies) when compared with most of the electrolyte resistances between elements. Interelement currents in the NC bar are quite small. Because of that, on

first approximation the overall behavior of the NC bar corresponded to that expected from the parallel combination of the individual segments of the NO bar.

The electrolyte resistance cannot be completely neglected. The low-frequency behavior of the NC bar showed an approximately constant phase angle (CPA) that deviated from 90° significantly more than in the case of the separate elements in the NO bar (compare Figures 8A and 8B). These deviations are likely to result not only from surface roughness [14] but also from macroscopically uneven distribution of the excitation current used in determining the impedance. Those portions of the working electrode closest to the counter electrode experience higher excitation than areas further away. The resulting finite transmission-line configuration creates an effective reduction of the phase angle [3,14]. The effect is expected to be greater when sampling the long NC bar, and then more marked when testing at the less conductive, dryer end of the bar. Both expectations are confirmed by the appearance of the impedance diagrams in Figure 8A. Because of these factors, an accurate convolution of the data from individual elements to predict the response of the composite bar should take the electrolyte resistance into account. This is attempted in a later section.

EIS Behavior, Active Macrocells.

The use of high-impedance current sources permitted observing wide differences in EIS behavior along the electrically continuous bars. The following discussion addresses the results from the two slabs where active corrosion was predominant.

Slab A1, NC bar (Figure 10)

The top element in the NC bar was a net electron consumer. The a.c.-isolated impedance diagram (Figure 10B, top) has the shape of a distorted semicircle. If the semicircle were due simply to the coupling of a charge-transfer resistance with an interfacial capacitance, the diameter of the semicircle would provide an indication of the reaction rate. Assuming for a moment that activation-limited oxygen reduction is the only operating reaction (Tafel constant bc~150 mV/decade [15]), the apparent semicircle diameter Rt~10 kohm yields a reaction current I=bc/2.3 Rt ~ 6.5 uA. This value is on the order of the 10.3 uA measured experimentally for the electronic current reaching that element.

The polarization conditions on the top element merit further consideration. The average current density on that electrode, based on the values discussed above and on the value of the surface area of the element, is on the order of 0.3 uA/cm^2. Assuming that this current density results solely from oxygen reduction at the metal surface, the corresponding flux of oxygen would be on the order of 8 10^{-13} mole/cm^2. This value is similar to the transport-limited flux of oxygen observed across several cm of a water-saturated concrete that had a composition comparable to the material used here [16]. However, as indicated earlier the transport of oxygen through dry concrete is expected to be orders of magnitude faster than through the water-saturated material [10]. Activation control, rather than transport control of the oxygen-reduction reaction appears then to be more likely in the present case.

The shape of the impedance diagram (Figure 10B, top diagram) can be examined in the light of this interpretation. The impedance of a reduction reaction subject to mixed activation-diffusion polarization is expected to have the form [17,18,19]:

$$Zr=bc/2.3\ I + [bo/(2.3(Il-I)]\ \tanh(\sqrt{j\ u})/\sqrt{j\ u} \qquad (7)$$

with $u=2\pi f d^2/D$ (8)

where I is the reaction current, Il is the limiting current, d is the effective diffusion distance and D is the diffusion coefficient. The frequency-dependent part of Eq.(7) is a finite-diffusion-length Warburg impedance [20]. This term, by itself, has an impedance diagram with a 45° slope at the high frequency end, while the impedance converges toward the real axis at the low frequency limit [18,19,20]. This behavior matches the appearance of the experimental diagram, but the total impedance must include the activation term bc/2.3 I and also the contribution of the interfacial capacitance. When those factors are taken into consideration the total impedance at the high frequencies no longer corresponds to a 45° slope in the impedance diagram, but one would expect instead a vertical line dominated by the capacitive term [19,20]. The results have been tentatively interpreted by assuming that the experimental 45° slope at the high frequencies is due to uneven current distribution effects in the high resistivity medium, giving rise to a transmission-line behavior [1,3,21]. In line with the previous arguments, the frequency-dependent term is assumed to be small in magnitude compared with the activation term. This seems to be consistent with the value observed for the frequency at which the imaginary component of the impedance was highest (~0.01 Hz). Assuming that this results from parallel coupling between an activation term of ~10 kohm and an interfacial capacitance, the latter would be about 50uF/cm^2, which is on the order of the values estimated earlier. Experiments are in progress to test this interpretation.

The electronic currents entering and leaving the second element from the top in this bar are almost equal. The isolated impedance diagram (second from top, Figure 10B) shows an almost straight line with a slope of about 40°. The magnitude of the impedance was found to be roughly inversely proportional to the square root of the test frequency. However, because of the arguments indicated above, it is difficult to explain that behavior as resulting from a simple diffusional impedance. The potential-time trends in the NO bar (Figure 6) indicated that active metal dissolution can take place at the level of this element, so the negligible net current does not exclude rapid, balanced cathodic and anodic reactions taking place. The element is located in a region where the concrete resistivity should change rapidly along the length of the bar. Since the reference electrode dimensions are also comparably large, the observed behavior could be modeled as resulting from excitation current distribution effects. There is not enough information to decide on the appropriate model.

The element just above the water line had low frequency impedance values that were one to two orders of magnitude smaller than those at the other elements in the same bar. The ac-isolated impedance diagram of this element (Figure 10B, bottom) does not correspond to the simple combination of a charge transfer resistance with an interfacial capacitance. The low phase angle suggests highly uneven distribution of the excitation current [1]. This could be due to factors including the macroscopic electrode arrangement, crevices between corroding steel and concrete aggregate particles (or isolation material between elements) [22], or the presence of finely distributed semiconductive corrosion products [21,23]. The lowest frequency used (~1mHz) is not enough to disclose whether the impedance will converge toward a real value at the low frequency limit. The overall low magnitude of the impedance suggests nevertheless that significant Faradaic activity was taking place at this element. It was the strongest net electron generator in the macrocell, but the rate of metal dissolution may significantly exceed the equivalent of the external macrocell current since some oxygen reduction at the element surface is also possible [16].

The fully immersed element had at the time of the measurements very small galvanic

interaction with the rest of the bar. The isolated impedance diagram suggested a dominant capacitive component. It would appear that charge-transfer processes were taking place at a rate much smaller than in the element immediately above. Because of water saturation, oxygen reduction should be taking place at a low rate in this element, leaving slow metal dissolution as the likely predominant reaction taking place. Previous measurements in this element [5,6] showed that at exposure times of ~300 days there was a strong galvanic interaction with the rest of the system. At that time the element was a net electron generator. The area of highest corrosion in this macrocell appears then to have drifted to the next element up during the intervening period. The drift may have resulted from the increasing accumulation of chlorides above the waterline, facilitating anodic dissolution there.

Impedance convolution model

The impedance diagrams for the composite NC bar (Figure 10A) have generally different appearance from those obtained under individual a.c. isolation. The diagrams measured with the three lower test electrode arrangements show roughly the same value of impedance magnitude and phase angle at the lowest test frequencies. The upper diagram has low frequency impedance magnitudes typically an order of magnitude higher than the others.

A model has been tentatively formulated (see Figure 13) to convolute the EIS data from the isolated elements into a predicted response for the composite bar. In that Figure, Z1 to Z4 represent the independent impedance of each of the four elements of the now continuous bar, which is represented by the grounded conductor at left. Points 1 to 4 represent the positions of the four reference electrodes. For simplicity, it is assumed that the excitation current in each impedance test of the composite bar is generated at the point where the corresponding reference electrode is placed. R1 to R4 are the equivalent resistances of the concrete between each reference electrode and the bar. Za, Zb and Zc represent the impedance of the reinforced concrete between each pair of element levels (as it will be shown below, it was necessary to assume more than a simply resistive path between levels). Zt1 to Zt4 is the value of the impedance of the composite measured when placing a counter electrode next to each of the corresponding reference electrodes.

Since the current is assumed to originate at each indicated node, the impedance of the composite bar is simply that of the resulting ladder array. Thus for example the impedance measured from node 1 is:

$$Zt1 = 1/At1 \qquad (9)$$

with:

$$At1 = \frac{1}{R1+Z1} + \frac{1}{Za + \dfrac{1}{\dfrac{1}{R2+Z2} + \dfrac{1}{Zb + \dfrac{1}{\dfrac{1}{R3+Z3} + \dfrac{1}{Zc+R4+Z4}}}}} \qquad (10)$$

Similar relationships, with appropriate modifications, were derived for nodes 2 through 4.

The values of R1 to R4 and Za to Zc were obtained by considering the isolated impedance behavior of the elements at the high frequency limit. Under those conditions Z1 through Z4 should be negligible because the interfacial capacitance admittance is very high. The limit values shown in Figure 10A in parenthesis correspond to a frequency of 1kHz (very high frequency features, if present, were judged to be the result of spurious wiring capacitances). The values of R1 to R4 were then equated to the four corresponding experimental high frequency limit values. Za to Zc were assumed to be purely resistive at the high frequency limit. The corresponding values Ra through Rc were evaluated by solving the system of equations based on Eq.10 when Z1 through Z4 are zero and R1 through R4 are known. Notice that there is a redundant equation since there are only three unknowns. The results obtained by using the data from R1, R2 and R3 were very similar to those obtained using R1, R2 and R4. The latter set, used for further calculations returned the values Ra=3200 ohm, Rb=134 ohm and Rc=243 ohm. Notice that these values, once combined with the reference electrode/element resistances, are in rough agreement with the point-to-point results shown in Figure 7.

Solution of the system of equations based on Eq.10, but using only the resistive limits of Za through Zc, provided predicted values that were too low for the low-frequency impedance magnitudes measured. As a result, it was postulated that Za through Zc had a frequency-dependent component [23] which was modeled as a reactive component. This was implemented using the model in Figure 14. An idealized section of reinforced concrete contains an isolated length of steel bar (as in the disconnected elements in the slab during the impedance tests). Assuming that electrode reactions are negligible, at low frequencies the steel does not offer a conductive path and the impedance of the section is resistive and equal to Rh+Re. At very high frequencies the interfacial capacitance of the bar offers a zero impedance path, shunting Re; the section impedance is resistive and with a value Rh. At intermediate frequencies the current is shared between Re and the bar, which is assumed for simplicity to be equivalent to capacitances 2C near each end. The impedance of the segment is then modeled by

$$Zs=Rh + 1/(1/Re + j\ 2\pi\ f\ C) \qquad (11)$$

This model was implemented assuming generally similar behavior for Za, Zb and Zc, taking Rh=Re and using a nominal value C=.004 F (which is on the order of the apparent interfacial capacitance of the longer segments).

The system of simultaneous equations based on Eq. 10 was then solved numerically for Zt1 through Zt4, using data from Figure 10B at eight selected test frequencies ranging from 100 Hz to 0.0009 Hz. Results of the predicted composite response are shown in Figure 15 arranged similarly to the data in Figure 10B (the experimental values are represented by the fainter dotted line). The calculations predict quantitatively the main features and magnitude ranges of the observed response. The low frequency impedance magnitude at the first, second and fourth levels (counting from the top) reflects the coupling to the low-impedance element just above the water line. The top level measurements show still relatively high impedance upon coupling, because the resistance of the concrete at that level is high and less of the excitation current reaches the lower levels. The convolution model confirmed most of these expectations as well as some details. For example, the phase angle for the level just above the water is higher in the coupled bar, since the interfacial capacitance of the other elements introduces a larger reactive component. The model

failed to reproduce the high frequency arch observed at the second level from the top in Figure 3.7, as well as fine structure at the high frequencies. This is not surprising, since the model treats the individual impedances as located at discrete points, and the coupling network is a gross simplification of the continuous, heterogeneous structure of the slab.

Slab A1, NO bar (Figure 11)

The top element in this bar showed evidence of a period of active corrosion earlier (see Figure 6) but was passive again at the time of the EIS tests. Accordingly, the response approached the capacitive behavior seen in the passive elements of slab P1. The bottom element was corroding actively, judging from the low static potential. Since there is no coupling to the rest of the bar, oxygen reduction needs to proceed by slow diffusion through the water-saturated concrete and the overall corrosion rate is expected to be low. As in the lowest element in the NC bar of the same slab, the impedance response shows a capacitive character, which would suggest that the admittance of charge-transfer processes is small and consequently that the corrosion current is low. This interpretation may require assuming relatively large values for the apparent interfacial capacitance of the active segments in the submerged zone [24,25]. The two intermediate segments in this bar show a low-angle impedance response. Corrosion at those levels was seen to proceeds at a sizable rate in a duplicate specimen (see Reference [5]) but interpretation of the impedance spectrum is difficult as discussed earlier.

Slab A2, NC bar (Figure 12)

The macrocell current pattern and the a.c-isolated impedance behavior of the elements in this bar suggest that corrosion is proceeding at a high rate only at the lowest element. To examine the a.c.isolated diagram of that element, a depressed semicircle can be visually fitted to the diagram. The diameter (about 1 kohm) is assumed to correspond to a charge-transfer resistance. Taking a B constant of 26 mV [26] one obtains a nominal corrosion current of 26 uA, which is larger than but on the order of the observed net electronic flow leaving the element (10.1 uA). Post-test examination of specimens exposed under similar conditions [5] revealed also rough agreement between magnitudes obtained in this manner and the directly observed mass loss.

The intermediate elements were net electron consumers, as was the top element. The latter shows a response resembling that of the top element in the NC bar of slab A1 (the high-frequency end of the spectrum, starting at about 100 Hz, was complicated by parasitic elements and only the data below 100 Hz are shown in Figure 12A). The magnitude of the impedance of the top segment at the low frequencies was higher than in the case of slab A1, perhaps reflecting the lower current flow (4.5 vs 10.3 uA).

The response of the composite electrode is strikingly similar at all four test levels, and very close in magnitude and shape to that observed for the lowest element when tested under a.c.-isolation. This is not surprising when the counter electrode geometry is taken into consideration. Unlike in the tests reported in Figure 10, the counter electrode here runs along the full length of the composite working electrode. In terms of the model in Figure 13, the impedances Za to Zc are approximately equal to zero. Therefore, the response at all four levels should be the same and equal to the parallel combination of the four individual impedances. Since the impedances of the upper three elements are much higher than Z4, the overall impedance is close to Z4. The four tests in Figure 12A were taken immediately following each other. The test for the lowest element shown in Figure 12B was taken on a different date. The

impedance of the composite should have been about 10% smaller in magnitude at the lowest frequencies but is only about 3% smaller. Small day-to-day variations preclude accurate verification of the model predictions in this case.

CONCLUSIONS

1. Macrocell currents developed on steel-reinforced concrete slabs that were partially submerged in a high chloride environment.

2. The impedance of individual segments of electrically continuous bars was measured by using a.c.-isolation with high impedance current sources.

3. The macrocell conditions resulted in highly differentiated EIS behavior along the reinforcing steel.

4. Segments where oxygen reduction was predominant provided results that suggested that the reaction was activation-limited in relatively dry concrete.

5. A model for convoluting the results from individual steel segments was used to predict the EIS response of the entire, interconnected bar. The impedance magnitude at low frequencies was predicted to decrease following interconnection. The extent of the predicted magnitude reduction depended on the concrete admittance between elements. The main trends predicted by the model were confirmed experimentally.

6. EIS measurements of passive bars revealed predominantly capacitive behavior. The impedance of passive composite bars behaved as the simple parallel combination of the individual segments but appeared to show the effects of uneven excitation current distribution.

ACKNOWLEDGMENT

This work was supported by the Materials Office, Florida Department of Transportation, in cooperation with the U.S. Department of Transportation. The opinions, findings and conclusions expressed here are those of the authors and not necessarily those of the supporting agencies.

BIBLIOGRAPHY

1. M. McKubre, "Techniques for AC Impedance Measurements in Corrosion Systems", Paper No.480, Corrosion/87, NACE, Houston, 1989.

2. J. Slater, "Corrosion of Metals in Association with Concrete", ASTM STP 818, ASTM, Philadelphia, 1983.

3. D.Macdonald, M.McKubre and M.Urquidi-Macdonald, Corrosion, Vol.44, p.2 (1988).

4. N.Buenfeld, J.Newman and C.Page, Cement and Concrete Research Vol 16, p.511 (1986)

5. A.Aguilar, A.Sagues and R.Powers, "Corrosion Measurements of Reinforcing Steel in Partially Submerged Concrete Slabs", in Corrosion Rates of Steel in Concrete, N.Berke, Ed., STP 1065, ASTM, Philadelphia, 1990.

6. A.Aguilar, "Corrosion of Reinforcing steel in Prtially Submerged Concrete", M.S. Thesis, University of South Florida, Tampa, Florida (1988).

7. R. Kessler and R. Powers, Interim Report "Corrosion Evaluation of Substructure, Long Key Bridge", Corrosion Report No. 87-9A, Materials Office, Florida Department of Transportation, Gainesville, Florida , 1987.

8. A.Zayed, A.Sagues and R.Powers, "Corrosion of Epoxy-Coated Reinforcing Steel", Paper No. 379, Corrosion/89, National Association of Corrosion Engineers, Houston, 1989.

9. A.Sagues, "Evaluation of Corrosion Rate by Electrochemical Impedance in a System with Multiple Polarization Effects", Paper No.25, Corrosion/89, National Association of Corrosion Engineers, Houston, 1989.

10. K. Tuutti, "Corrosion of Steel in Concrete" (ISSN 0346-6906), Swedish Cement and Concrete Research Institute, Stockholm (1982)

11. C.Page "Basic Principles of Corrosion" in Corrosion of Steel in Concrete, p.3, P.Schiessl, Ed., RILEM Report 60-CSC (ISBN 0412 32100 9), Chapman and Hall, London (1988).

12. F.Mansfeld, Corrosion Vol. 44, p.856 (1988).

13. Matthew Thomas, "Effect of Surface Roughness on the Double Layer Capacitance at The Steel/Alkaline Medium Interface", M.S. Thesis, University of South Florida (1988)

14. R.DeLevie, Electrochimica Acta, Vol.9, p.1231 (1964).

15. H. Kaesche, "Metallic Corrosion", p.166, National Association of Corrosion Engineers, Houston (1985)

16. O. Gjorv, O.Vennesland and A. El-Busaidy, Materials Performance, Vol.25, No.12, p.39 (1986).

17. S. Haruyama, "Faradic Impedance of Mixed Potential Electrode," Proc. Fifth Int. Cong. Metallic Corrosion, p.82, National Association of Corrosion Engineers, Houston (1974).

18. T. Tsuru, "Treatment of Diffusion Impedance in AC Impedance Method", 61st. Japan Soc. Corr. Eng. Symposium Report, pp.97-106 (1985).

19. A. A. Sagues, Corrosion Vol 44, 555 (1988).

20. D.Macdonald and M. McKubre "Electrochemical Impedance Techniques in Corrosion Science",in Electrochemical Corrosion Testing, p.110, ASTM STP 727, F. Mansfeld and U.Bertocci, Eds,. ASTM, Philadelphia (1981).

21. J. R. Park and D. D. Macdonald, Corrosion Sci Vol 23, 295 (1983).

22. A. Sagues, " Evaluation of Corrosion Rate by Electrochemical Impedance in a System with Multiple Polarization Effects", Paper No.25, Corrosion/89, National Association of Corrosion Engineering, Houston, (1989).

23. R. Oltra and M.Keddam, Corrosion Sci. Vol.28, p.1 (1988).

24. J. Dawson, "Corrosion Monitoring of Steel in Concrete", in Corrosion of Reinforcement in Concrete Construction, A.Crane, Ed., Ellis Horwood, Chichester (1983).

25. S. Ehrlich and P. Moran, Corrosion, Vol. 45, p.689 (1989).

26. F.Mansfeld, "The Polarization Resistance Technique", in Advances in Corrosion Science and Technology, Vol. 6, M.Fontana and R.Staehle, Eds., Plenum Press, New York, 1976.

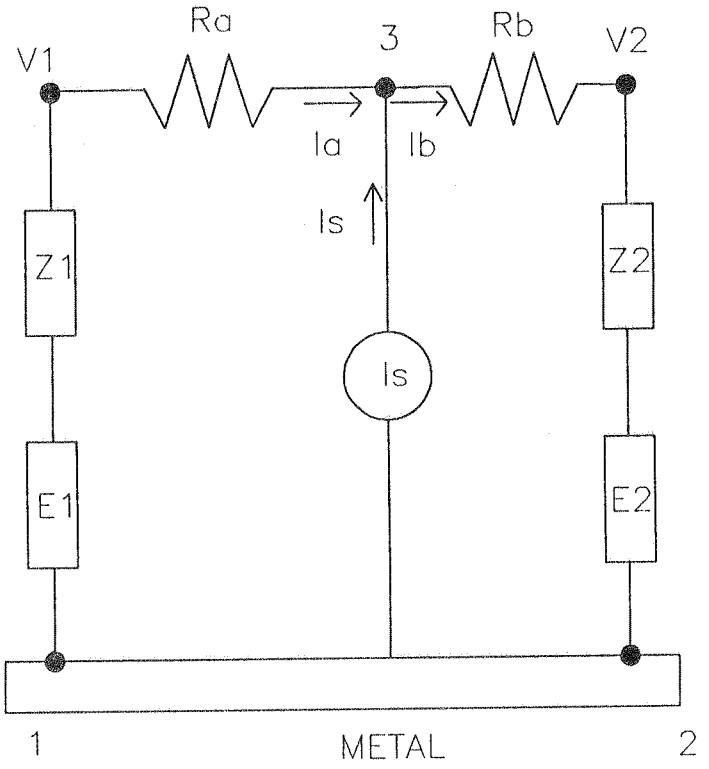

FIGURE 1 - A simplified, discrete corrosion macrocell.

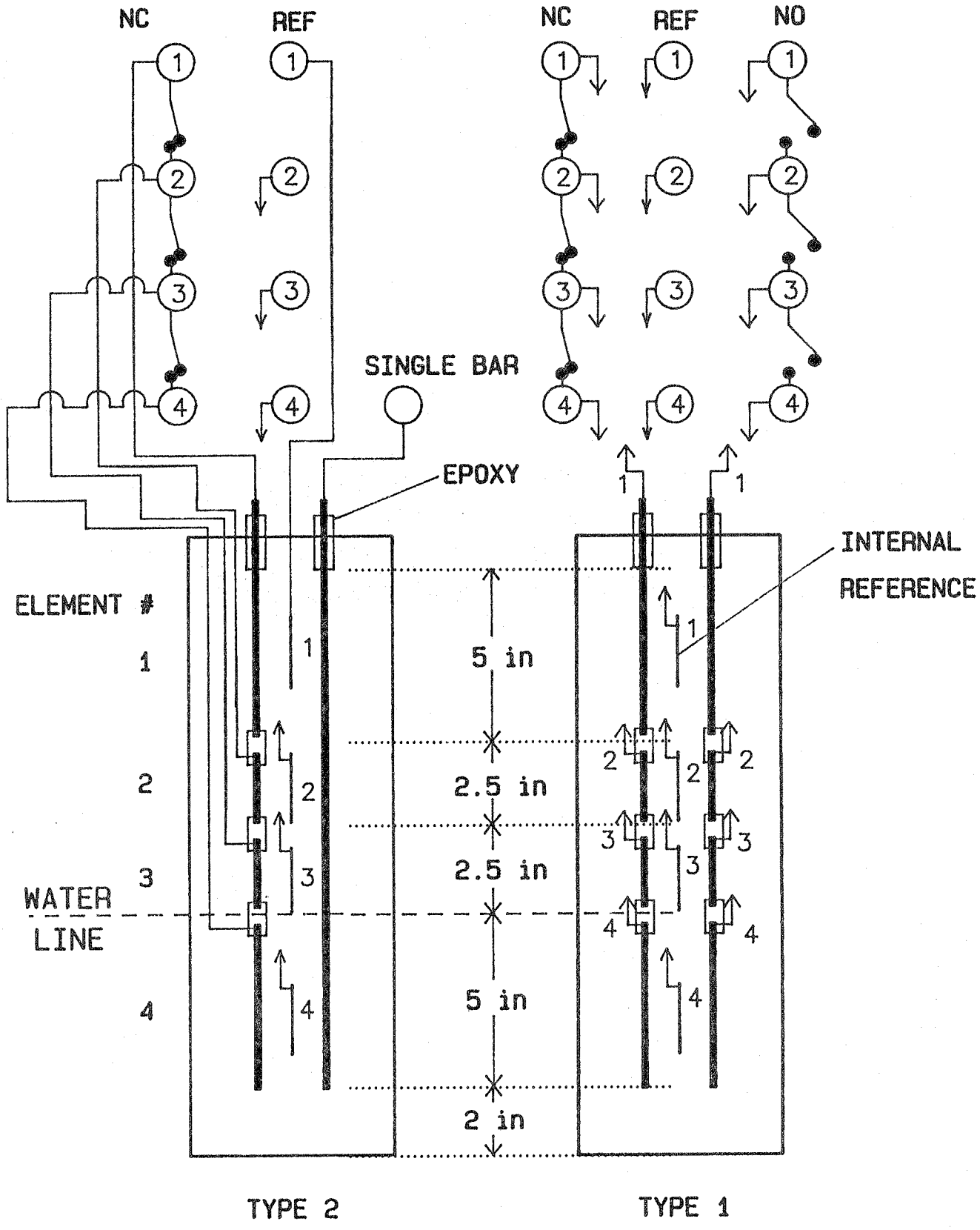

FIGURE 2 - Configuration of the multi-element reinforced concrete slabs selected for detailed EIS testing. (1 inch = 25.4mm)

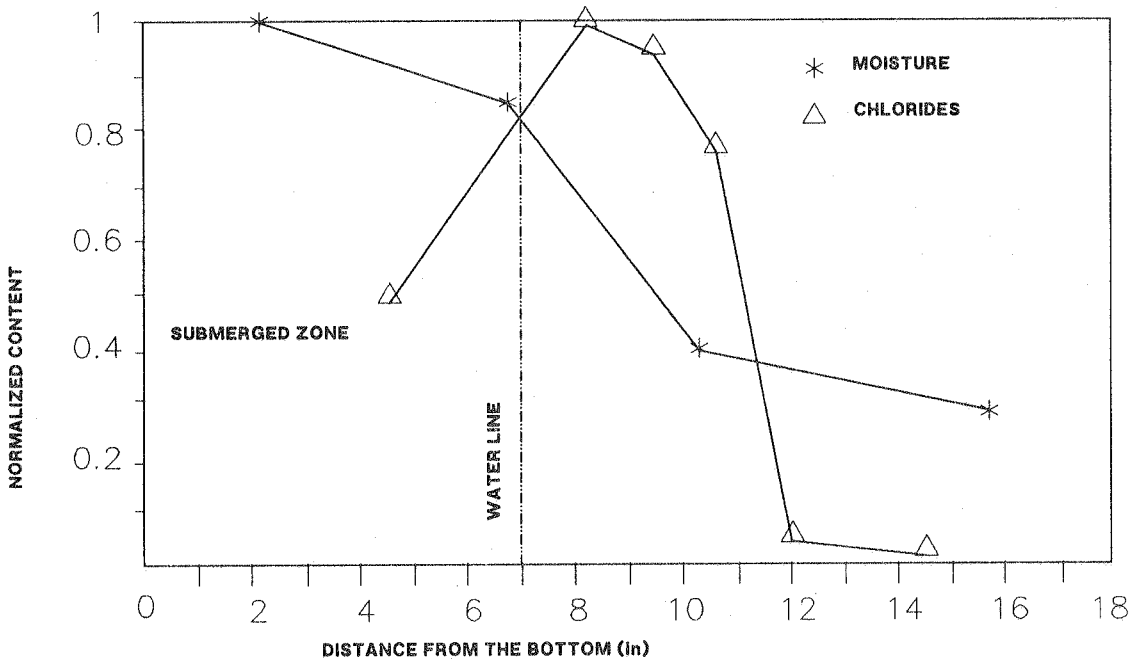

FIGURE 3 - Normalized chloride and water content profiles of a slab exposed for 300 days to a 9000 ppm chloride solution. The maximum chloride content was 16 Kg/m^3 of concrete (~26 pounds/cubic yard). Maximum moisture was 5.95 %, measured by evaporation at 60°C for 48 h. One inch equals 25.4 mm.[5]

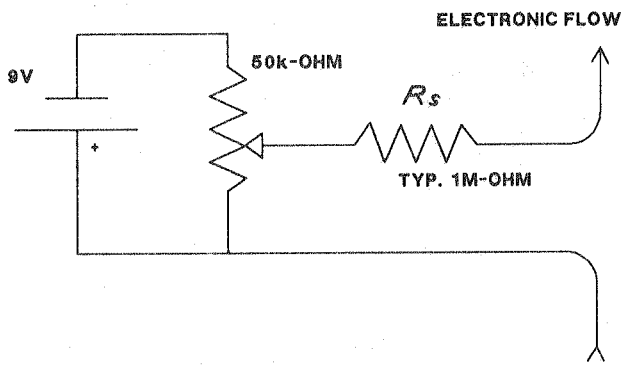

FIGURE 4 - Adjustable high impedance current source used to create a.c. isolation between rebar elements while maintaining the d.c. macrocell current flow. The source current was adjusted by means of the variable voltage divider. The current drain on the battery was low enough to provide drift-free performance during the impedance test.

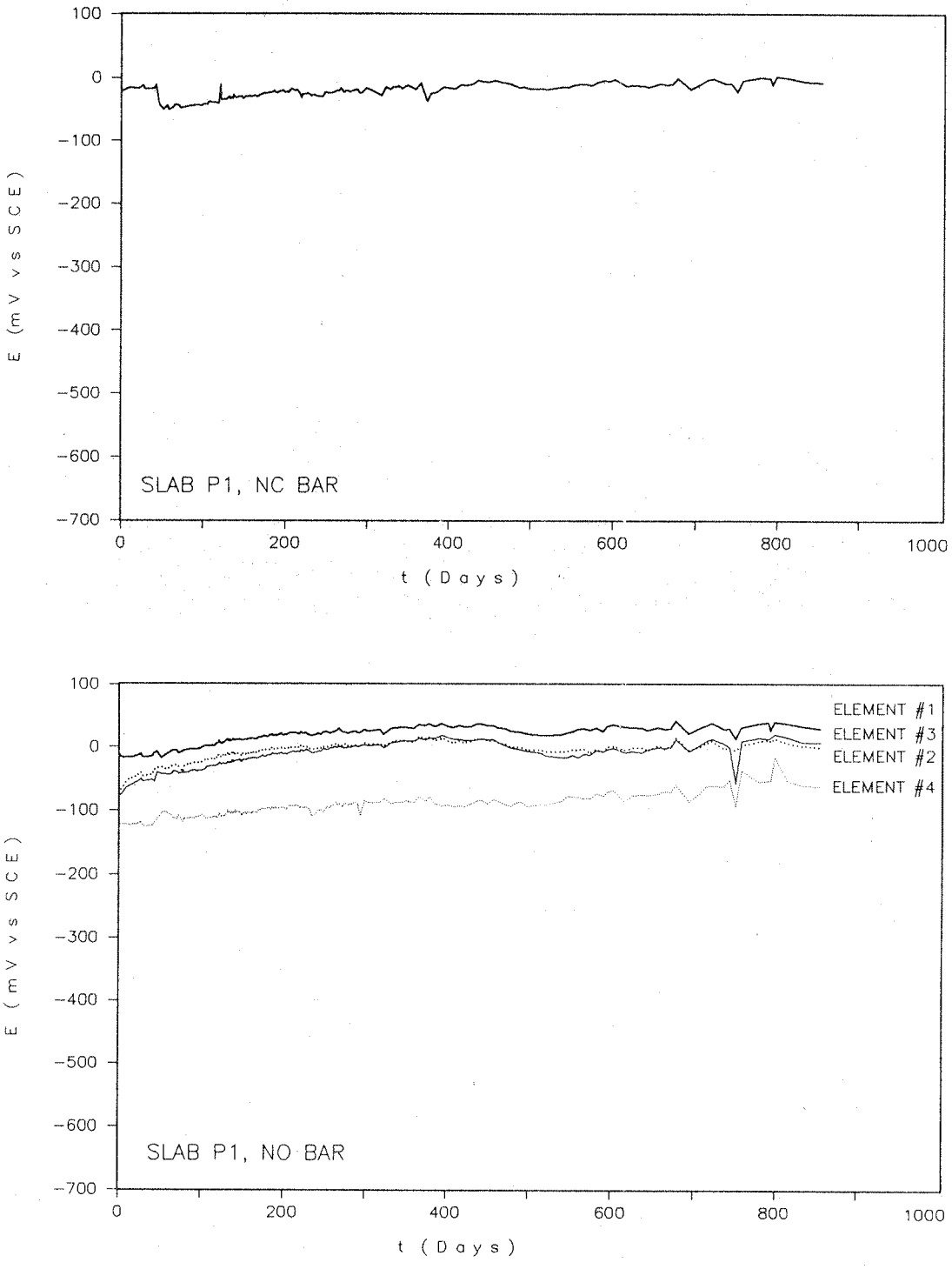

FIGURE 5 - Electrode potential of the composite NC bar (top) and individual elements in the NO bar (bottom) of slab P1 as a function of time. This slab was exposed to a liquid containing 300 ppm chloride. Individual elements are designated as per Figure 2.

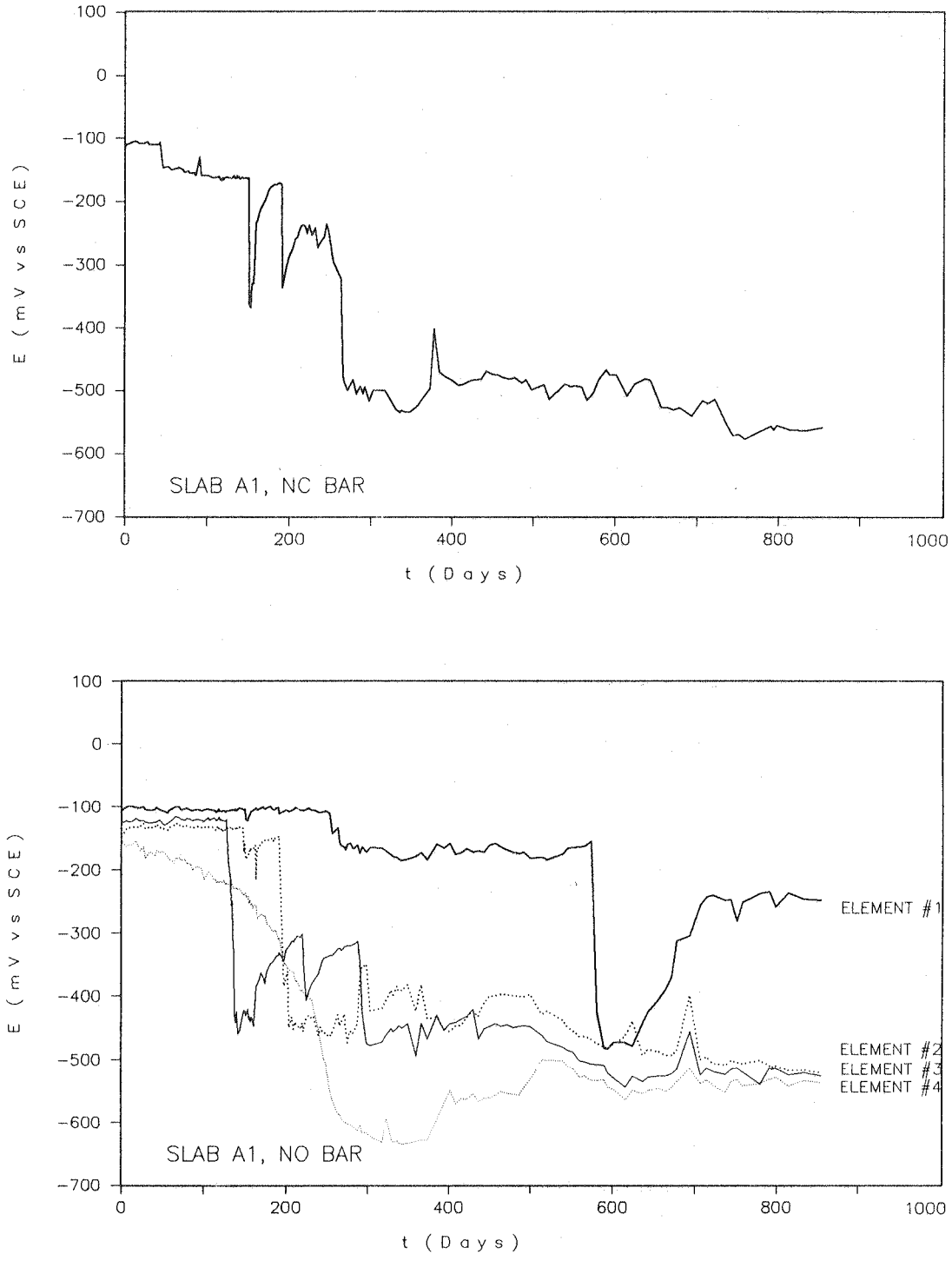

FIGURE 6 - Electrode potential of the composite NC bar (top) and individual elements in the NO bar (bottom) of slab A1 as a function of time. This slab was exposed to liquid containing 9000 ppm chloride. Slab A2 showed similar trends. Individual elements are designated as per Figure 2.

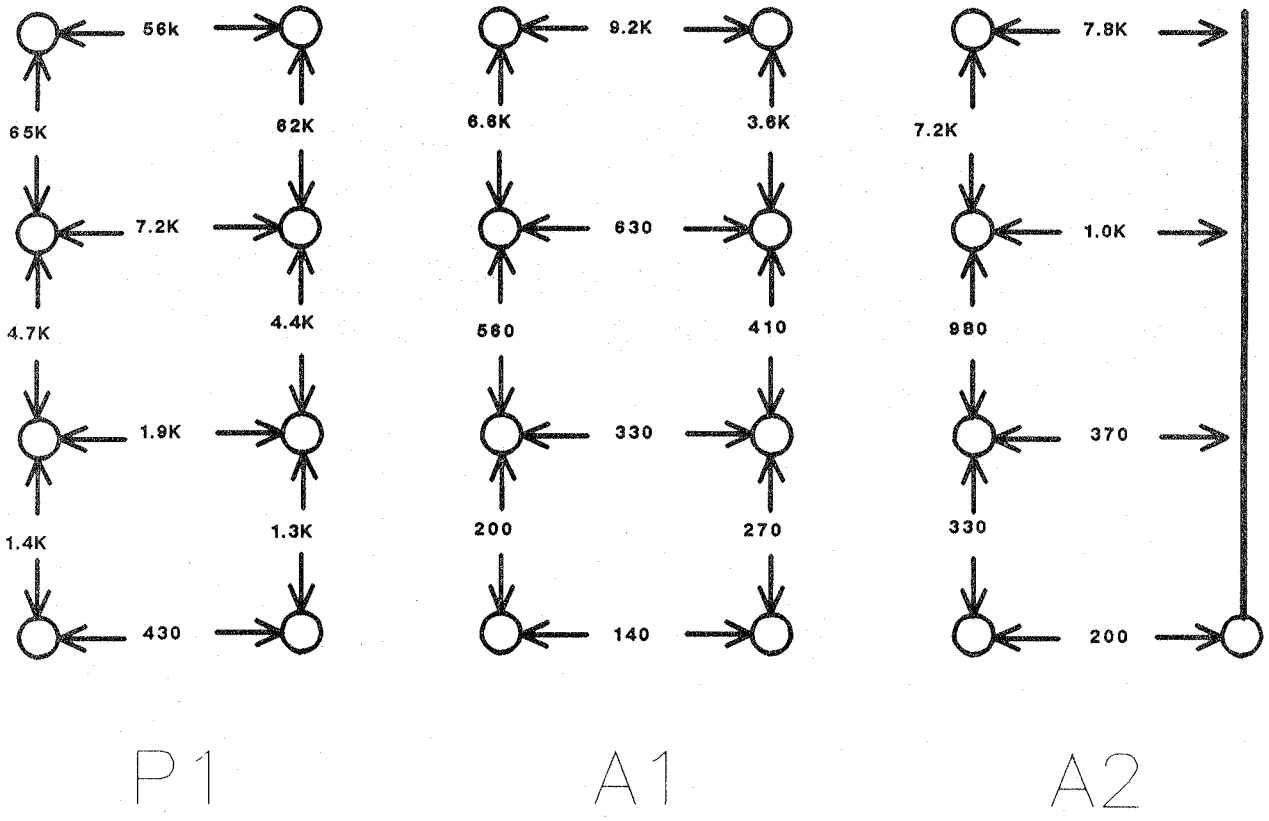

FIGURE 7 - Point-to-point a.c. resistance between rebar terminals of slabs P1, A1 and A2 after 900 days of testing. All values are in ohms. Measurements were taken with all switches opened. The connections to the bar segments are arranged as per the schematic in Figure 2 , but the reference electrodes are not shown.

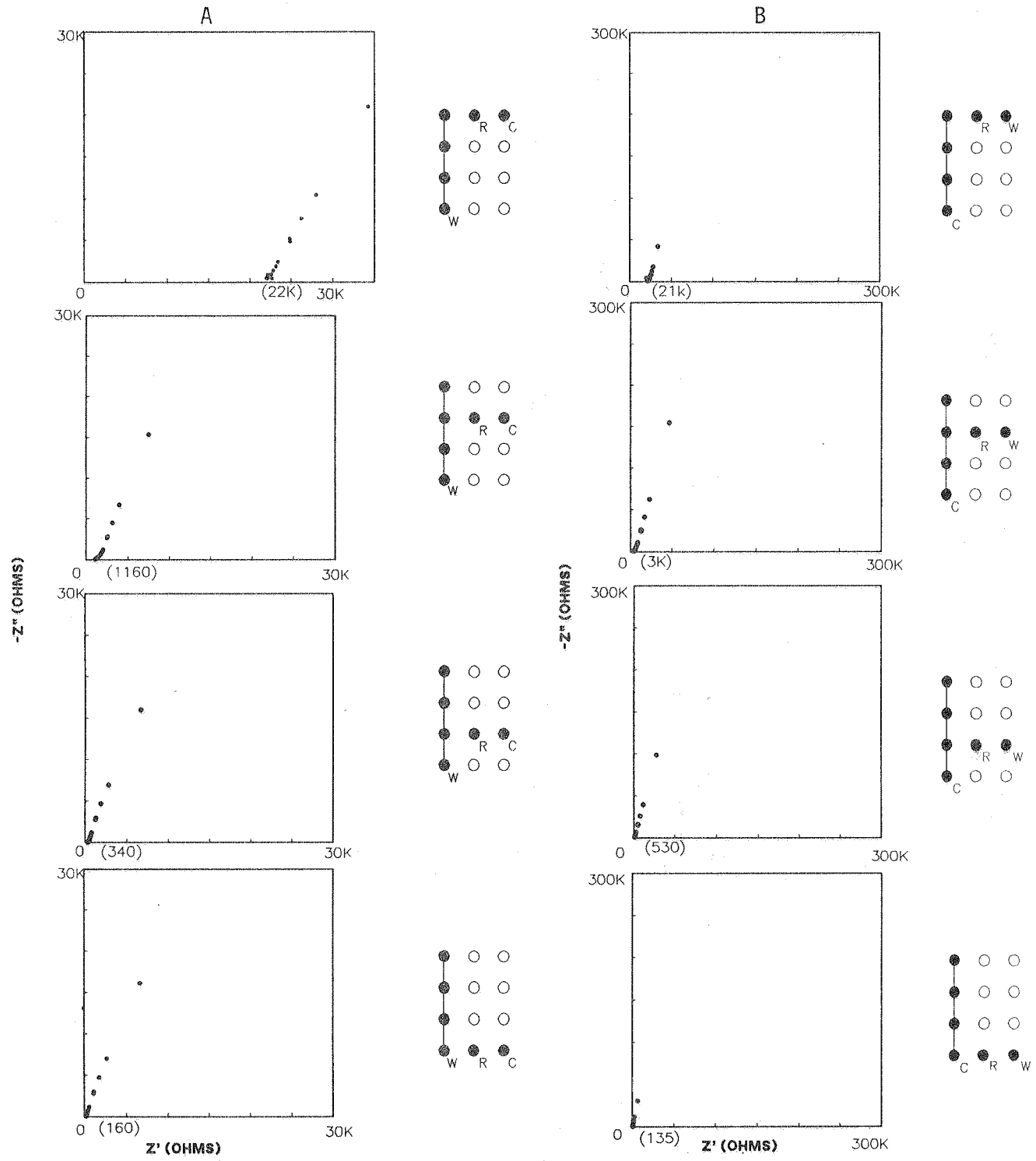

FIGURE 8 - A: EIS measurements of the NC bar in slab P1. The impedance diagrams are placed according to the position of the segments in the slab. The connection scheme is shown next to each diagram, keyed to Figure 2 (closed switches are represented by the short line joining terminals). The working, reference and counter electrode roles are shown by the initials. The lowest test frequency was 0.0009 Hz. Numbers in parenthesis denote the high frequency limit of the impedance magnitude.

B: EIS measurements of individual elements of the NO bar in slab P1.

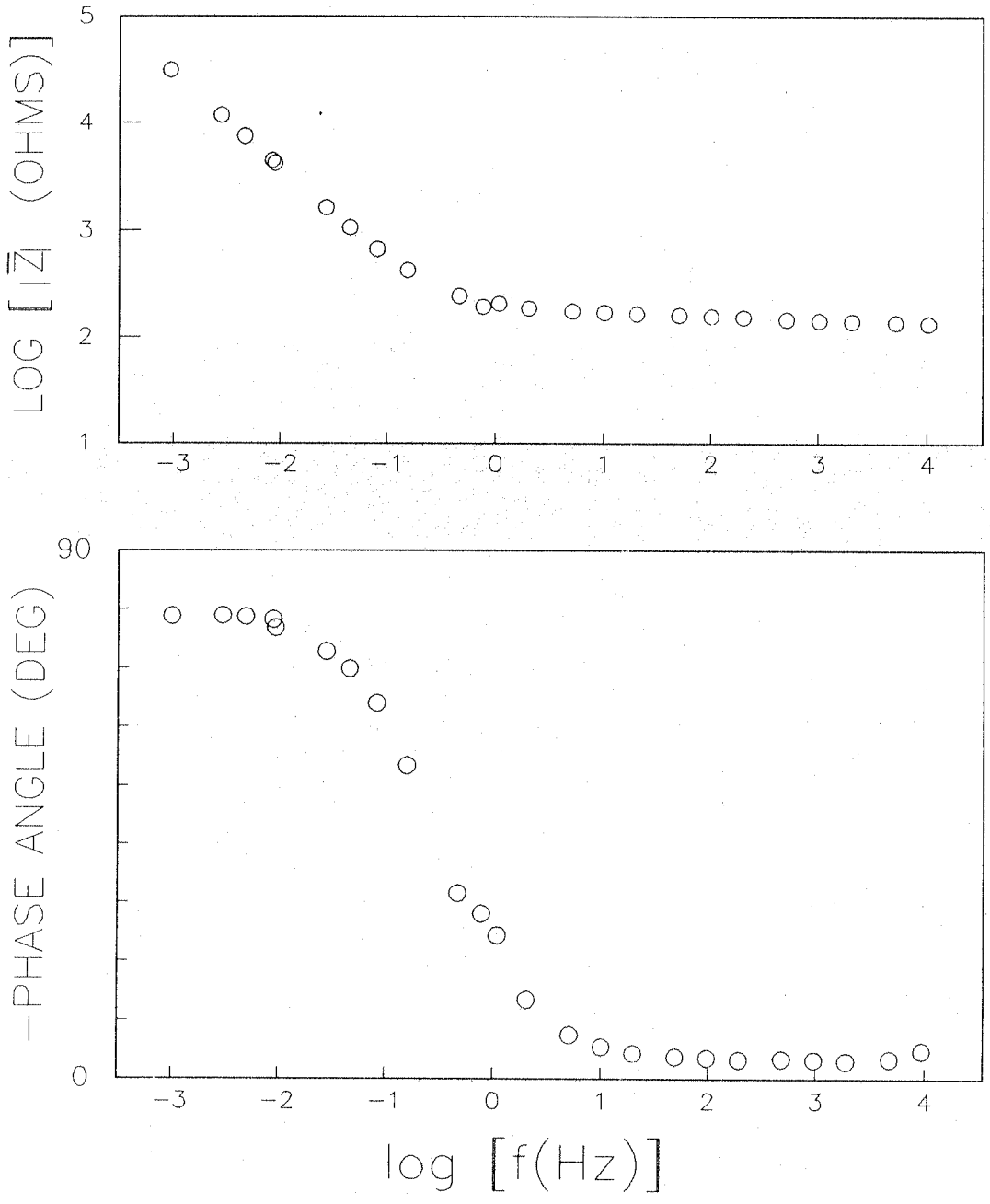

FIGURE 9 - Bode representation of the EIS behavior of a segment in slab P1 (NO bar, second from bottom).

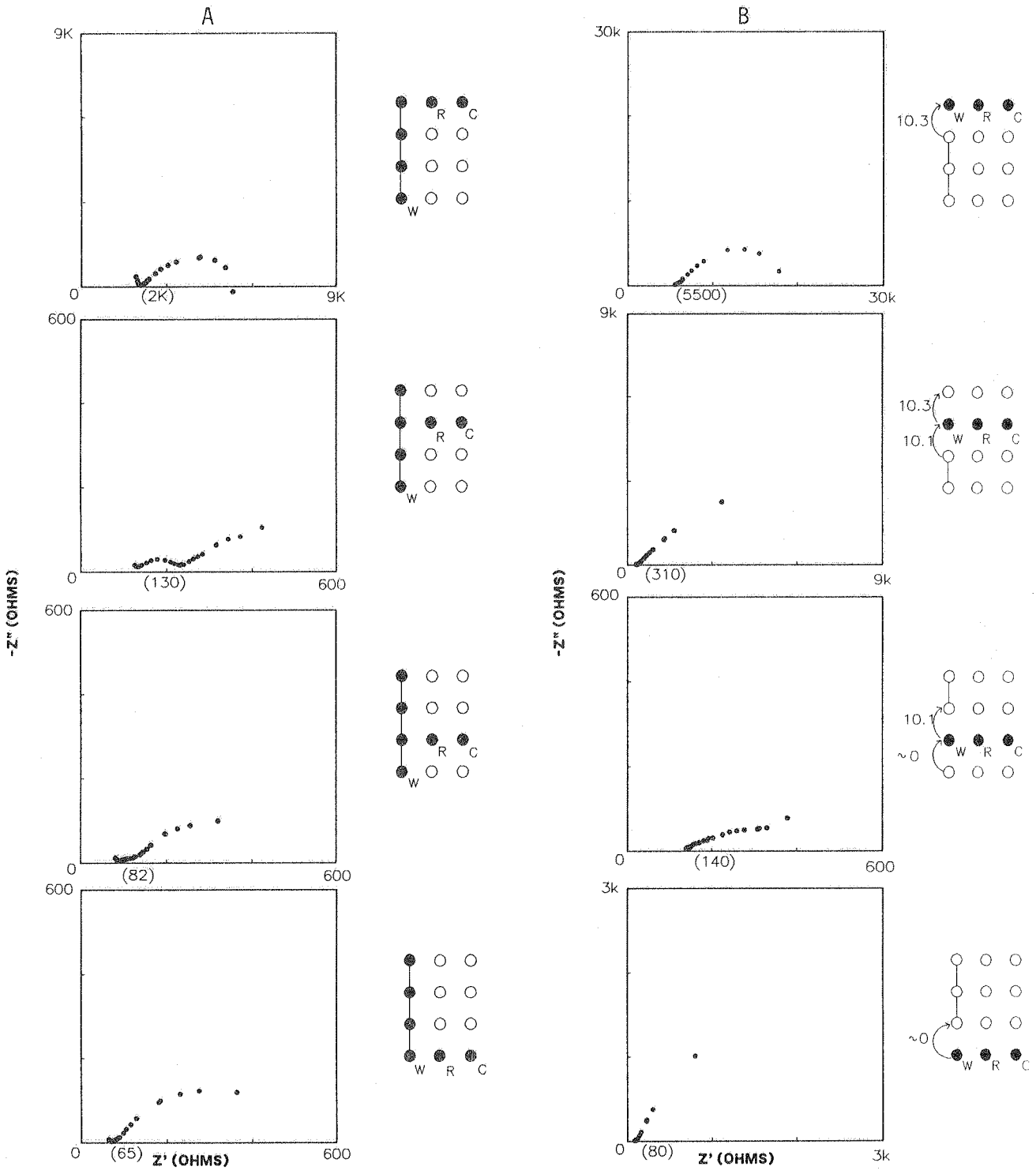

FIGURE 10 - A: EIS measurements of the NC bar in slab A1 using counter/reference electrode combinations at different levels. See figure 8 for notation.

B. EIS measurements of individual elements of the NC bar in slab A1. The element being tested is isolated form the others by current sources symbolized by the arrows. Electronic current direction and magnitude (in uA) are as shown.

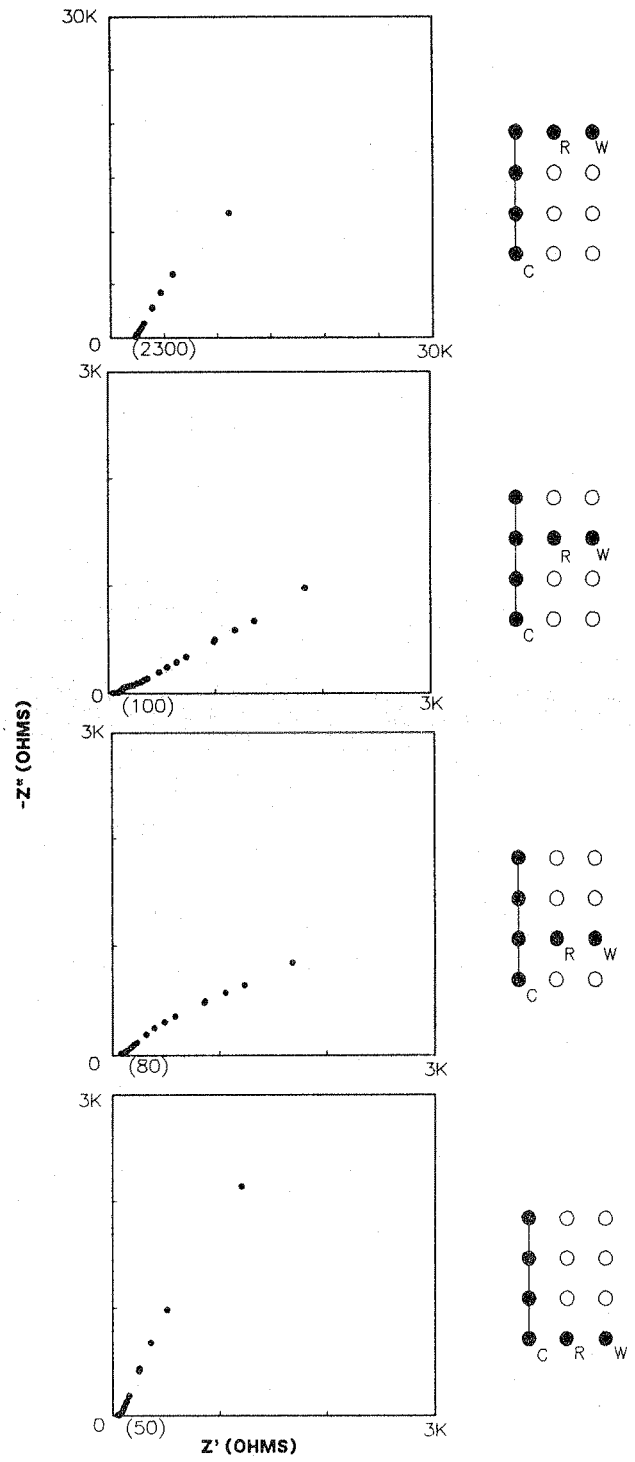

FIGURE 11 - EIS measurements of individual elements of the NO bar in slab A1, using the NC composite bar as the counter electrode. See Figure 8 for notation.

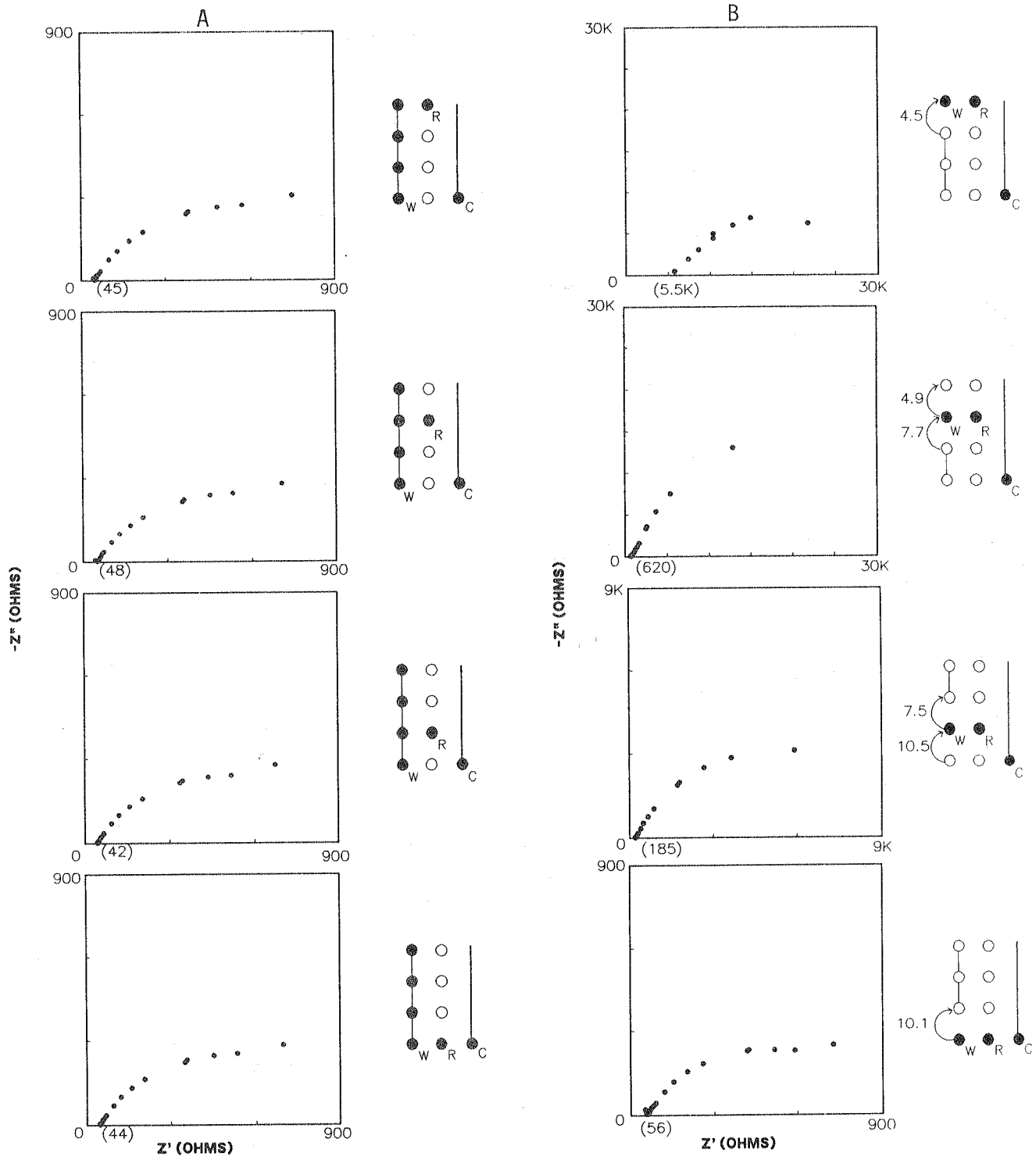

FIGURE 12 - A: EIS measurements of the NC bar in slab A2. The counter electrode is the physically continuous bar. See Figure 8 for notation.

B. EIS measurements of individual elements of the NC bar in slab A2. See Figures 8 and 10 for notation.

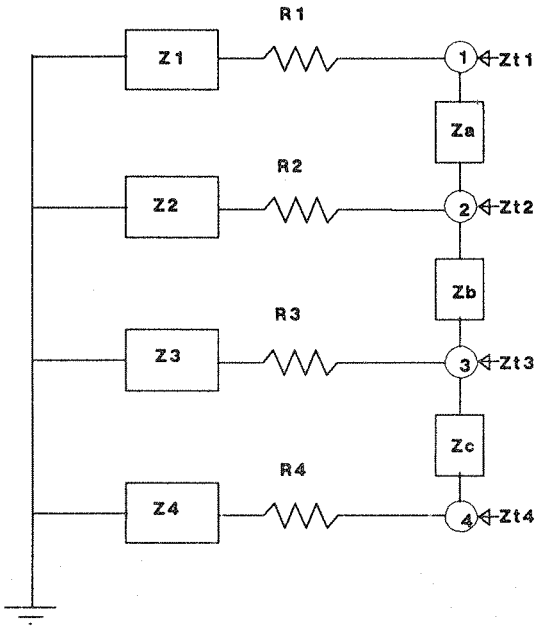

FIGURE 13 - Model used for the convolution of impedance data from individual segments.

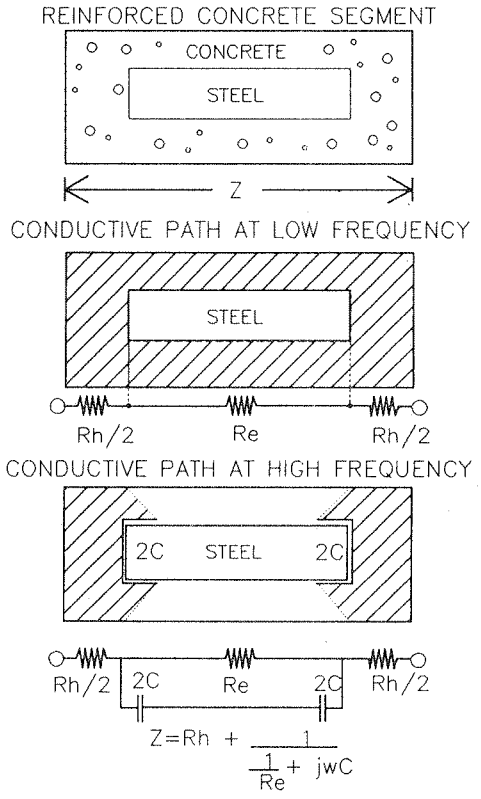

FIGURE 14 - Idealized current path (shaded region) and simplified impedance of a portion of reinforced concrete containing a passive, isolated steel bar.

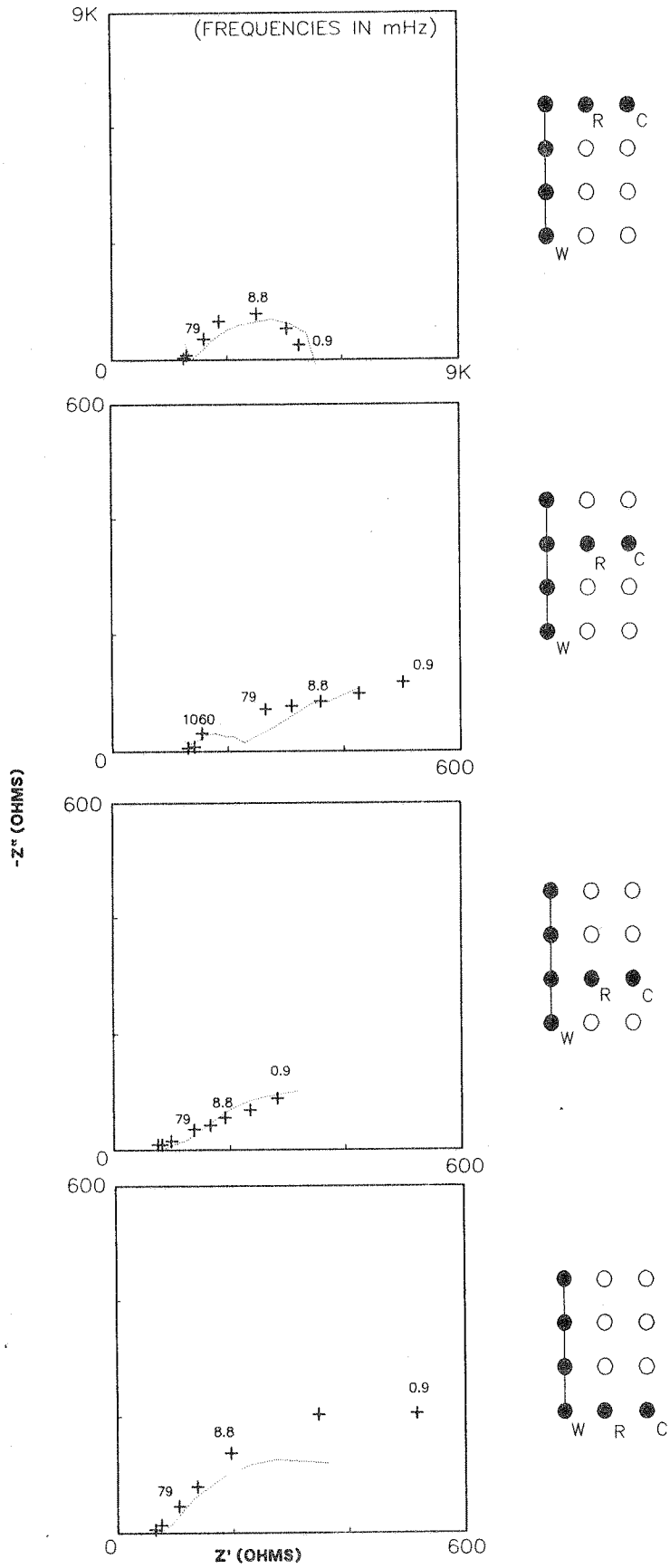

FIGURE 15 - Behavior of the NC bar of slab A1, as predicted (cross symbols) by applying the convolution model to the EIS measurements on a.c.-isolated segments. The actual measurements with the NC bar (Figure 10A) are shown here by the faint lines. See the previous Figures for notation.